NASA
Technical Memorandum 86933

USAAVSCOM
Technical Report 85-C-1

# Low Cycle Fatigue of MAR-M 200 Single Crystals at 760 and 870 °C



Walter W. Milligan
*Georgia Institute of Technology*
*Atlanta, Georgia*

N. Jayaraman
*University of Cincinnati*
*Cincinnati, Ohio*

Robert C. Bill
*Propulsion Laboratory*
*AVSCOM Research and Technology Laboratories*
*Lewis Research Center*
*Cleveland, Ohio*



Prepared for the
TMS-AIME Fall Meeting
Detroit, Michigan, September 17-19, 1984

NASA

# LOW CYCLE FATIGUE OF MAR-M 200 SINGLE CRYSTALS AT 760 and 870 °C*

Walter W. Milligan
Georgia Institute of Technology
Fracture and Fatigue Research Laboratory
Atlanta, Georgia 30332

N. Jayaraman
University of Cincinnati
Department of Metallurgical Engineering
Cincinnati, Ohio 45221

and
Robert C. Bill
Propulsion Laboratory
AVSCOM Research and Technology Laboratories
Lewis Research Center
Cleveland, Ohio 44135

## SUMMARY

Fully reversed low cycle fatigue tests were conducted on single crystals of the nickel-base superalloys Mar-M 200 at 760 and 870 °C. The plastic strainrange was held constant, but the orientations of the tensile axes of the specimens were varied. The fatigue behavior was found to be orientation-dependent.

At 760 °C, planar slip (octahedral) lead to orientation-dependent strain hardening and cyclic lives. Multiple slip crystals strain hardened the most, resulting in relatively high stress ranges and low lives. Single slip crystals strain hardened the least, resulting in relatively low stress ranges and higher lives. A preferential crack initiation site which was related to slip plane geometry was observed in single slip orientated crystals.

At 870 °C, the trends were quite different, and the slip character was much more homogeneous. As the tensile axis orientation deviated from <001>, the stress ranges increased and the cyclic lives decreased. Two possible mechanisms were proposed to explain the behavior: one is based on Takeuchi and Kuramoto's cube cross-slip model, and the other is based on orientation-dependent creep rates.

E-2444

## INTRODUCTION

Mar-M 200 is a nickel-base superalloy developed in the 1960's for turbine blade applications. Although originally used in the conventionally cast form, it represents the first generation of alloys identified for potential application in the directionally solidified and single crystal forms (refs. 1 and 2). Several modifications have since been made in modern single crystal blade alloys, including the elimination of the grain boundary strengthening elements such as carbon, boron, and zirconium (ref. 3), all of which are present in Mar-M 200.

---

*The electron microscopy was supported by NASA Lewis under Grant NSG-3506.

An inherent characteristic of single crystals that relates directly to blade design and performance is the anisotropy of physical and mechanical properties. It has been shown that the tensile and creep behavior of Mar-M 200 single crystals is a strong function of orientation and temperature (refs. 4 to 7). However, the behavior of the material under cyclic loading conditions is less thoroughly documented. Cube oriented crystals within 5° of <001> have been studied under cyclic loading at room temperature (ref. 8) and at elevated temperatures (refs. 9 and 10). Results from these studies are summarized below.

Crack initiation occurred at carbides (when carbon was present) and at micropores. At temperatures below 760 °C, fatigue lives were found to be a strong function of carbide size. The crack morphology was found to be dependent on slip character: at low temperatures, or intermediate temperatures and high frequencies, planar slip lead to Stage I (crystallographic) cracking; while at high temperatures, or intermediate temperatures and low frequencies, "wavy" slip lead to Stage II cracking perpendicular to the tensile axis. In some cases, Stage I propagation followed Stage II initiation. Under stress controlled conditions at room temperatures greater than 843 °C there was a strong effect of frequency; low frequencies resulted in extensive creep damage and low lives.

In these previous studies of the fatigue behavior, only the <001> orientation was investigated. The objective of the present study was to determine the effect of tensile axis orientation on the low cycle fatigue behavior of Mar-M 200 single crystals at 760 and 870 °C.

## MATERIALS AND PROCEDURE

The alloy chemistry is documented in table I. The alloy and microstructure have been described in detail previously (ref. 3). The single crystals were solution treated at 1220 °C for 2 hr and aged at 870 °C for 32 hr. The specimens were hollow cylinders, with nominal dimensions of an 8.25 mm i.d. by an 11.5 mm o.d., and a 12 mm gage length.

Tensile axis orientations were determined prior to testing by the Laue back reflection x-ray technique. These results are summarized in table II, and are also indicated on a standard stereographic triangle in figure 1. Elastic moduli for each specimen were measured mechanically prior to testing, and are presented in tables III and IV.

Low cycle fatigue tests were conducted on a closed-loop, servohydraulic system, in the longitudinal strain controlled mode. Cyclic frequency was 0.1 Hz. Specimens were heated by an RF induction unit, which resulted in a temperature gradient (radially and longitudinally) of ±2 C. Temperature was controlled manually, which resulted in a temperature variation of ±7 C.

Twenty-three fully reversed ($R = -1$) tests were conducted, 14 at 760 °C and 9 at 870 °C. The plastic strainrange ($\Delta\epsilon_p$) was held constant at approximately 0.08 percent for the majority of the tests. All but two specimens were cycled to failure, as numbers 27 and 51 were interrupted after several cycles for TEM deformation studies.

Representative samples were characterized fractorgraphically by both optical and SEM techniques. Deformation mechanisms were documented by the TEM. Foils were prepared for microscopy by grinding disks to a thickness of 0.075 mm, followed by ion milling until perforation. The ion milling process was observed to damage the microstructure, so the foils were then twin-jet electropolished for 5 sec to remove the damaged surface layer. Electropolishing was performed in a solution of 10 percent perchloric acid, 45 percent acetic acid, and 45 percent butyl cellusolve at 0 °C and 25 V. Foils were studied using a JEOL JEM 200 operating at 200 kV.

## RESULTS

### Heat Treated Microstructure

As shown in figure 2, the microstructure consisted of a bimodal distribution of primary and secondary $\gamma'$, with a large $\gamma'$ size of approximately 0.5 to 1.0 μm, and a secondary $\gamma'$ size of approximately 0.1 to 0.3 μm. The microstructure also contained large MC type carbides (fig. 2(a)), submicroscopic carbides, and a network of interfacial dislocations (fig. 2(c)). As figure 2(b) demonstrates, the $\gamma'$ size and volume fraction within the dendrite core were both significantly lower than in the interdendritic regions. There was also a slight variation in microstructure from specimen to specimen.

### Fatigue Behavior - 760 °C

Mechanical testing. - Nine tests were conducted at a nominal $\Delta\varepsilon_p$ of 0.08 percent, and four tests were conducted at higher $\Delta\varepsilon_p$'s. Experimental parameters are reported in table III, and the low $\Delta\varepsilon_p$ test parameters are also indicated in standard stereographic triangles in figure 3. As figure 3 illustrates, when the $\Delta\varepsilon_p$ was held constant but the tensile axis orientation was changed, other test parameters (total strainrange ($\Delta\varepsilon_t$), stress range ($\Delta\sigma$), and cyclic life ($N_f$)) varied significantly. Several trends can be identified. For the same $\Delta\varepsilon_p$, crystals near the major poles (<001>, <011>, and <111>) resulted in relatively high stabilized stress ranges and low lives. This behavior was most pronounced in crystals near the <111> orientation, followed by the <001> and <011> orientations. These are referred to as multiple slip orientations, because the resolved shear stress is the same on more than one octahedral plane, so more than one plane is favorable aligned for slip. Crystals orientated away from the major poles resulted in relatively lower stress ranges and higher lives. These are referred to as single slip orientations, because only one octahedral plane is favorably aligned for slip. The four tests that were conducted at higher $\Delta\varepsilon_p$'s followed the same trends, but the results are not included in figure 3.

Total strainrange varied independently of these trends, due to differences in elastic moduli. As shown in figure 4, there was a fairly good correlation between $\Delta\sigma$ and $N_f$. However, for the same $\Delta\varepsilon_p$ life varied by a factor of 10, and $\Delta\varepsilon_t$ did not correlate well with $N_f$.

Deformation analysis. - Figure 5(a) shows that the deformation microstructure after fatigue in a single slip crystal consisted of a parallel array of dislocation bands. Through detailed dislocation analysis (as described in the appendix), it was determined that the majority of these dislocations were

in the (111)[$\bar{1}$01] system, which is the primary octahedral slip system predicted by Schmid's law. Figure 5(b) shows the deformation microstructure after fatigue in a multiple slip crystal (near <001>), including three intersecting slip bands. It was determined that these bands contained dislocations on three different octahedral planes. Figure 6 shows a higher magnification series of micrographs of a slip band in this specimen, and is illustrative of the analysis method delineated in the appendix.

The interaction between the $\gamma'$ precipitates and the deformation dislocations was also examined. As shown in figures 6(f) and 7, the slip bands tended to cut through the $\gamma'$ precipitates during deformation. In some cases this $\gamma'$ shearing was accompanied by the generation of {100}<011> type dislocations in the superlattice, even in near <001> crystals (fig. 6). However, the majority of dislocations observed did lie on octahedral planes. Since both the octahedral plane dislocations within the slip bands and the cube plane dislocations next to the slip bands (in fig. 6) had the same burgers vector ([011]), it appears likely that the cube plane dislocations were generated by cross-slip from the octahedral planes.

Fractographic observations. - It was determined that the mechanisms of crack initiation and propagation were essentially independent of orientation in the ranges studied. Multiple crack initiation was observed at micropores (fig. 8(b)) and carbides, and propagation was observed to be in the Stage II mode.

One orientation effect was observed, however. In single slip and double slip crystals, macroscopically visible slip traces were generated on the specimen surface, as shown in figure 8, due to octahedral shear. The crack that lead to final failure always initiated at the apex of the ellipse formed by these slip traces. As illustrated in figure 9, this is the area where the stress component which is normal to a Stage I crack is at a maximum, thus facilitating early propagation. No slip traces were observed on the specimen surface in near <001> or <111> crystals, although fine slip bands were observed by the TEM.

## Fatigue Behavior - 870 °C

Mechanical testing. - Eight tests were conducted at a nominal $\Delta\varepsilon_p$ of 0.10 percent. Experimental parameters are reported in table IV, and are indicated in standard stereographic triangles in figure 10.

The fatigue behavior at 870 °C was also orientation dependent, but the trends were quite different from those observed at 760 °C. For the same $\Delta\varepsilon_p$, crystals oriented near <001> resulted in low stabilized stress ranges and high lives, while crystals orientated near <011> resulted in high stress ranges and low lives, and crystals oriented between these two extremes exhibited intermediate behavior. No specimens oriented near <111> were available for testing.

As shown in figure 11, there was a very good correlation between $\Delta\sigma$ and cyclic life. For the same $\Delta\varepsilon_p$, a high $\Delta\sigma$ resulted in a low life, while a low $\Delta\sigma$ resulted in a high life. Again, neither $\Delta\varepsilon_t$ nor $\Delta\varepsilon_p$ correlated well with life.

The initial constitutive behavior was also orientation-dependent. As shown in figure 12, crystals near <001> exhibited a stable stress range response from the first few cycles, while other orientations cyclically softened. Single slip crystals softened the most, while near <011> crystals softened to a lesser degree.

Deformation analysis. - At 870 °C, the deformation microstructure consisted of a very homogeneous, nonplanar dislocation arrangement (figs. 13 and 14), including a fairly high concentration of dislocations within the $\gamma'$ (fig. 13(b)). The most significant observation was that the deformation microstructure appeared to be independent of orientation. Both octahedral and cube plane dislocation segments were identified within the $\gamma'$, but the majority of dislocations present were nonlinear, and were not confined to a single plane.

Fractographic observations. - At 870 °C, all cracks initiated at surface connected and subsurface micropores, regardless of orientation (fig. 15). Propagation was in the Stage II mode, and was also independent of orientation.

## DISCUSSION

### Heat Treated Microstructure

The microstructure of the specimens tested in the present study was significantly different from the microstructures reported in previous studies for Mar-M 200 (refs. 5, 6, and 9). In the previous studies, the $\gamma'$ was reported to be uniform in size, approximately 0.3 μm on edge. In the present study, there was a bimodal distribution. The large $\gamma'$ varied between 0.5 to 1.0 μm in size, while the fine $\gamma'$ varied between 0.1 to 0.3 μm in size (fig. 2(c)). Piearcey et al. (ref. 2) have reported that a coarse dispersion of $\gamma'$ results when the alloy is slowly cooled from the solutionizing temperature, possibly explaining the bimodal $\gamma'$ size distribution in the present study.

The previous studies have also reported a relatively dislocation-free initial microstructure, while the specimens in the present study contained a fairly well defined interfacial dislocation network (fig. 2(c)). This is probably due to the coarsened $\gamma'$ size in the present study.

### Fatigue Behavior - 760 °C

At 760 °C, the fatigue behavior can be explained very well by Schmid's law. Multiple slip crystals deformed by dislocation glide on intersecting slip planes, which resulted in a high degree of strain hardening. In plastic strain controlled fatigue, this caused high stabilized stress ranges, low ductilities, and low lives. Single slip crystals deformed by dislocation glide on a single slip plane, which resulted in a higher degree of slip reversibility, a lower degree of strain hardening, and therefore higher ductilities and higher lives. The observed dislocation microstructure (fig. 5) support these conclusions.

For a constant plastic strainrange in single crystals of various orientations, the stress range is an important parameter for two reasons. First, the stress range is the dominant factor in crack propagation, and second, the stress range can be a qualitative indicator of the relative ductility when

planar slip is active. Wright and Anderson (ref. 11) have shown that the maximum tensile stress, rather then the plastic strainrange, is life limiting in several directionally solidified nickel-base superalloys.

The near <111> crystal resulted in the highest stress range, which is consistent with its low octahedral Schmid factor and its high yield strength (ref. 4) at this temperature. The fatigue behavior of the remaining crystals was consistent with the number of active slip planes. The best fatigue resistance (under plastic strain control) was observed in single slip crystals, followed by the near <001> crystals (double slip), followed by the near <001> crystal (quadruple slip), respectively. The cyclic lives also correlated well with monotonic tensile ductility trends reported by Kear and Piearcey (ref. 4) at this temperature, with the exception of the <011> orientation. Based on the relatively high tensile ductility that was reported for <011> crystals, the cyclic lives in the present study appear to be low. This discrepancy near <011> may be explained by the fact that this orientation degenerates from double slip to single slip under monotonic tension due to lattice rotation, but should remain a stable double slip orientation under fully reversed fatigue cycling.

It should be noted that the observed trends are a direct result of the type of fatigue test that was employed, and vastly different trends would be obtained under stress controlled or total strain controlled cycling.

### Fatigue Behavior - 870 °C

At 870 °C for the same plastic strainrange, crystals near <001> resulted in low stress ranges, crystals near <011> resulted in high stress ranges, and crystals between the two exhibited intermediate behavior. Cyclic life correlated very well with stress range. However, it is difficult to rationalize the fatigue behavior mechanistically. There are three possible reasons for the observed orientation-dependent stress ranges: different deformation mechanisms, differences in strain hardening or softening behavior, and differences in yield strengths.

Since the deformation microstructure was independent of orientation, it is likely that the active deformation mechanisms were independent of orientation. The microstructure consisted of a wavy, homogeneous dislocation structure (figs. 13 and 14), which is a result of extensive climb and cross slip (ref. 12). This type of deformation microstructure has been documented for Mar-M 200 tested in tension at 843 °C (ref. 12), in creep at 857 °C (ref. 7), and in low stress fatigue at 843 °C (ref. 10). Since cross slip is relatively easy at this temperature, every orientation exhibited multiple slip behavior, so the orientation dependence should have been less pronounced than it was at lower temperatures. This was the case in the present study. However, some orientation dependence was still evident.

The second factor that can influence the cyclic stress range is the difference in the softening behavior. The orientation-dependent softening that was observed in figure 12 tended to reduce the differences in stress range between the <001> and the <011> crystals during the first 10 percent of the life, but it cannot explain the final, absolute differences in stress ranges between the different orientations.

The third factor that can influence the stress range is the possibility of differences in the yield strengths (both tensile and compressive). Because of the way in which the plastic strain controlled fatigue test was conducted (by slowly increasing the total strain range until the desired plastic strain range was attained), initial yield strengths were not available. However, since the plastic strain ranges in the present study were small (about 0.1 percent), a reasonable first order approximation of relative strength could be $\Delta\sigma/2$. This would represent a yield strength average at 0.05 percent offset, and would incorporate both tensile and compressive strengths. Using this approximations, it can be seen that the <011> and singe slip oriented crystals were approximately 25 percent stronger than the <001> crystals during the first few cycles (fig. 12). Based on Schmid's law and assuming octahedral plane slip, the yield strengths of the <001> and <011> crystals should be identical. This was not the case, but it is not uncommon for superalloys to exhibit a deviation from Schmit's law, especially at elevated temperatures.

Kear and Piearcey (ref. 4) and Copley et al. (ref. 5) have shown that Mar-M 200 single crystals orientated near <111> and <011> exhibit tensile yield strengths which are lower than <001> oriented crystals at about 760 °C. Copley and Kear demonstrated the same type of behavior in $Ni_3Al$ $\gamma'$ single crystals in the same temperature regime (ref. 13). In all three cases, the reason for the suppressed yield strengths in the <011> and <111> orientations was shown to be the initiation of slip on the primary cube planes in the superlattice. This mechanism of lowering the yield strength near <011> cannot be directly applicable to the present study, because the <011> crystals had higher yield strengths than the <001> crystals. Obviously, other mechanisms are important at 870 °C as compared to 760 °C.

Kear and Piearcey also tested Mar-M 200 single crystals in tension at 982 °C (ref. 4), and found that <011> crystals had slightly higher yield strengths than <001> and <123> crystals. The difference was fairly small (about 7 percent), but the direction of the trend agrees qualitatively with the yield strength/orientation trends in the present study. This may indicate that similar mechanisms are active at both 870 and 982 °C. Unfortunately, no physical mechanisms were proposed to explain the observed orientation dependence of the yield strength at 982 °C. In a more recent study, Giamei (ref. 14) studied the compressive yield strengths of PWA 1444 Alloy single crystals at 891 °C. This alloy is chemically similar to Mar-M 200, except for the lack of Co, B, Zr, and C. He reported that the compressive yield strengths of <011> oriented crystals were 17 percent higher than the <001> oriented crystals. Not only is this trend in the same direction as in the present study, but the relative magnitudes of the differences in yield strengths are also similar. Once again, no mechanisms were postulated to explain the observed behavior.

Since the deformation behavior of the $\gamma'$ phase is extremely important in controlling the deformation of Mar-M 200 (ref. 13), studies of the deformation behavior of single phase $L1_2$ intermetallics can help develop a possible explanation for the observed yield strength trends, both in the present study and in the previously mentioned studies (refs. 4 and 14). Takeuchi and Kuramoto (ref. 15) showed that the critical resolved shear stress (CRSS) for octahedral slip in $Ni_3Ga$ depended on the RSS on the cube cross slip plane, up to about 500 °C. A high RSS on the cube cross slip plane aided cross slip of the leading superpartiales, resulting in dislocation pinning and an increased yield strength. Lall et al. (ref. 16) showed that the yield strength

of <011> oriented single crystals of single phase $Ni_3$ (Al,Nb) was significantly higher than the yield strength of <001> oriented crystals, up to about 630 °C. The Takeuchi-Kuramoto (T-K) theory was able to explain this behavior, and with slight modifications, Lall et al. (ref. 16) and Ezz et al. (ref. 17) were able to explain other apparently contradictory orientation-dependent behavior. On first glance, it would appear that the T-K model may be directly applicable to the present study, because the yield strength increased linearly with the increasing RSS on the cube cross-slip plane (fig. 16). However, there is a problem in directly applying the pure intermetallic model; the cube cross-slip mechanism was shown to be important only at temperatures below the peak flow stress temperature, where octahedral slip dominated the deformation. Above the peak temperature, deformation was controlled by primary cube slip in orientations away from <001>. Since Kear and Piearcey (ref. 4) were able to show primary cube slip and a yield strength maximum at 760 °C in <011> Mar-M 200 crystals, it appears certain that the transition point has already been reached for Mar-M 200 and 870 °C. Under this assumption, the T-K cross-slip model would no longer be directly applicable. However, their model can be modified slightly to account for the observed yield strength behavior of Mar-M 200 single crystals.

The T-K model accounts for two basic temperature regimes in single phase $L1_2$ intermetallics: below the peak flow stress temperature, where primary planar octahedral slip dominated; and above the peak flow stress temperature, where primary planar cube slip dominated. In Mar-M 200, however, there are actually three temperature regimes of interest: below the peak, where primary planar octahedral slip dominates; above the peak temperature but below about 843 °C, where primary planar octahedral slip and primary planar cube slip both operate; and at high temperatures (above about 843 °C), where 'wavy,' non-planar, thermally activated slip dominates. The region of interest here is the third one. In this temperature regime, every orientation exhibited multiple slip, including slip on the octahedral systems. Therefore, cube cross-slip could act as an important strengthening mechanism in this regime, just as it does at lower temperatures. This can explain the increasing yield strengths of Mar-M 200 crystals as the orientation deviated from <001> at temperatures greater than about 843 °C.

Another way of looking at the theory shows that it is not really a modification at all. It could be assumed that cube cross-slip is an important hardening mechanism wherever octahedral slip operates within the $\gamma'$ of a superalloy. The only reason that the strengthening effect is not observed in near <011> and near <111> crystals in a very limited temperature regime (about 650 to 800 °C, depending on orientation and composition) is that primary cube slip has a larger, negative effect. The cross-slip mechanism would therefore be present whenever there is slip occurring on octahedral planes, but it may be obscured by other phenomena, such as primary cube slip or strain hardening under some conditions.

Since there is no direct evidence available at the present time which would support the above discussion beyond a reasonable doubt, there is a possibility that other mechanisms may be responsible for the observed fatigue behavior. Another mechanism which may possibly explain the orientation-dependent yield strengths of Mar-M 200 single crystals above about 843 °C is discussed below.

Leverant et al. (ref. 12) have demonstrated that the yield strength of Mar-M 200 is a strong function of strain rate (up to 100 percent/min) at temperatures greater than 843 °C. The reason for this strain rate dependence was that time dependent plastic flow (creep) can occur in this temperature regime, thus reducing the offset yield strength. It has also been shown that the creep behavior of this alloy is very orientation-dependent at 843 °C (ref. 7), although a limited number of orientations was tested. If it could be shown that the <001> orientation results in a higher creep rate than the <011> orientation at 870 °C, this could help explain a lower yield stress (and necessarily a lower stress range in plastic strain controlled fatigue) for <001> crystals when compared to <011> crystals. This is especially pertinent to the present study, because the cyclic frequency was slow (0.1 Hz), resulting in a relatively low average strain rate of only 10 percent/min. Unfortunately, no data are available to support or refute this possibility, although several related studies may provide some insight.

Shah (ref. 18) tested $Ni_3Al$ $\gamma'$ single crystals in compressive creep at 982 °C, and showed that the minimum creep rate of the <001> orientation was about twice the minimum creep rate of the <011> and <123> orientations. If these results are related to Mar-M 200 deformation at 870 °C, they would support the above theory. Giamei (ref. 14) tested PWA 1444 single crystals in both tensile and compressive creep at 891 °C in both <001> and <011> orientations. He found that the minimum creep rate in compression was twice as high for <001> crystals as compared to <011> crystals, but the minimum creep rate in tension was twice as high for <011> crystals as compared to <001> crystals. Obviously, the evidence is mixed, so the above creep-related theory is still very speculative.

## General Comments

The above discussion has shown that the orientation dependence of the LCF behavior of Mar-M 200 single crystals is very sensitive to temperature. As illustrated by figure 17, the relative fatigue "resistance" of any orientation with respect to another changes as the temperature changes from 760 to 870 °C. This is a direct result of a change in basic deformation behavior at about 800 °C.

It should also be clear that the relative fatigue "damage" is a complex function of temperature, orientation, strain level, strain rate, and stress level. Without a basic understanding of deformation mechanisms under relatively simple monotonic loading, it would be extremely difficult to understand fatigue behavior, and almost impossible to predict it. Therefore, if we want to continue to develop our understanding of high temperature fatigue, we must continue to strive to completely characterize and understand fundamental metallurgical deformation mechanisms in these alloys.

## CONCLUSIONS

At 760 and 870 °C in plastic strain controlled fatigue, single crystals of Mar-M 200 exhibited orientation-dependent behavior which can be summarized as follows:

1. At 760 °C, octahedral planar slip lead to orientation-dependent stress ranges and cyclic lives. Multiple slip crystals strain hardened the most, resulting in relatively high stress ranges and low lives. Single slip crystals strain hardened the least, resulting in lower ranges and higher lives. Cyclic lives correlated well with stress ranges and previously reported tensile ductilities.

2. At 870 °C, homogeneous, nonplanar slip was observed. Stress ranges increased and lives decreased as crystal orientations deviated from <001>. The mechanisms responsible for this behavior are unclear at the present time, but two possible contributing factors are cube plane cross-slip within the $\gamma'$, and the possibility of orientation-dependent creep rates.

3. At both temperatures, fatigue lives correlated closely with stress range under the conditions of imposed inelastic strain.

4. The orientation dependence was a strong function of temperature.

## APPENDIX A

## DISLOCATION ANALYSIS

From diffraction theory (ref. 19), a dislocation will be "invisible" under the two-beam conditions that satisfy the equation

$$\underline{g} \cdot (\underline{b} \times \underline{u}) = 0$$

where $\underline{g}$ is the diffraction vector, $\underline{b}$ is the burgers vector, and $\underline{u}$ is the line direction. Residual contrast will result if

$$\underline{g} \cdot \underline{b} = 0$$

The line direction can be determined by measuring the angle $\theta$ between the $\underline{g}$ vector and the apparent (two-dimensional) line direction. Unless the dislocation is of a pure screw nature, $\underline{b}$ and $\underline{u}$ will lie on the same plane, defined as the slip plane.

As an example, the two dislocations marked in figures 6(a) to (d) were analyzed. Dislocation contrast resulted under $\underline{g} = [020]$, $[\bar{2}20]$, and $[220]$, for which $\theta = 0°$, 49°, and 41°, respectively. The line direction was therefore [010], for which $\theta$ should have been 0°, 45°, and 45° (ideally).

The dislocations disappear under $g = [\bar{1}\bar{1}1]$ and [200]. Therefore

$$\underline{b} = \underline{g}_1 \times \underline{g}_2, \text{ or } [011]$$

Since $\underline{b} \neq \underline{u}$, the dislocation is not of a pure screw character, and the slip plane is defined as $\underline{b} \times \underline{u} = (100)$. The dislocations are therefore in the [011] (100) system.

## REFERENCES


1. J.M. Oblak and B.H. Kear: Electron Microscopy and Structure of Materials, pp. 566-616, Univ. of California Press, Berkeley, 1972.

2. B.J. Piearcey, B.H. Kear and R.W. Smashey: ASM Trans. Q., 1967, vol. 60, pp. 634-645.

3. M. Gell, D.N. Duhl and A.F. Giamei: Superalloys 1980, pp. 205-214, American Society for Metals, Metals Park, Ohio, 1980.

4. B.H. Kear and B.J. Piearcey: Trans. Metall. Soc. AIME, 1967, vol. 239, pp. 1209-1215.

5. S.M. Copley, B.H. Kear and G.M. Rowe: Mater. Sci. Eng., 1972, vol. 10, pp. 87-92.

6. G.R. Leverant and B.H. Kear: Metall. Trans., 1970, vol. 1, pp. 491-498.

7. G.R. Leverant and B.H. Kear: Metall. Trans., 1973, vol. 4, pp. 355-362.

8. M. Gell and G.R. Leverant: Trans. Metall. Soc. AIME, 1968, vol. 242, pp. 1869-1379.

9. G.R. Leverant and M. Gell: Trans. Metall. Soc. AIME, 1969, vol. 245, pp. 1167-1173.

10. G.R. Leverant and M. Gell: Metall. Trans. A, 1975, vol. 6, pp. 367-371.

11. P.K. Wright and A.F. Anderson: Superalloys 1980, pp. 689-698, American Society for Metals, Metals Park, Ohio 1980.

12. G.R. Leverant, M. Gell and S.W. Hopkins: Mater. Sci. Eng., 1971, vol. 8, pp. 125-133.

13. S.M. Copley and B.H. Kear: Trans. Metall. Soc. AIME, 1967, vol. 239, pp. 9 -984.

14. A.F. Giamei: PWA-FR-12637, Pratt and Whitney Aircraft Group, East Hartford, CT, Nov. 1979. (AD-A080088.)

15. S. Takeuchi and E. Kuramoto: Acta Metall., 1973, vol. 21, pp. 415-425.

16. C. Lall, S. Chin and D.P. Pope: Metall. Trans. A, 1979, vol. 10, pp. 1323-1332.

17. S.S. Ezz, D.P. Pope and V. Paidar: Acta Metall., 1982, vol. 30, pp. 921-926.

18. D.M. Shah: Scripta Metall., 1983, vol. 17, pp. 997-1002.

19. M.H. Loretta and R.E. Smallman: Defect Analysis in Electron Microscopy, Wiley, New York, 1975.

TABLE I. - Mar-M 200 ALLOY COMPOSITION

| Element | Wt % |
|---|---|
| Ti | 2.05 |
| Al | 5.00 |
| Nb | 1.00 |
| Cr | 9.20 |
| Co | 10.40 |
| W | 12.60 |
| Fe | 0.30 |
| Zr | 0.05 |
| C | 0.15 |
| B | 0.02 |
| Ni | Bal. |

TABLE II. - SPECIMEN ORIENTATIONS

| Test temperature | Number | Degrees from | | |
|---|---|---|---|---|
| | | <001> | <111> | <011> |
| 760 °C | 32 | 4 | 51 | 42 |
| | 25 | 5 | 40 | 40 |
| | 14 | 40 | 14 | 30 |
| | 45 | 44 | 33 | 2 |
| | 19 | 38 | 33 | 8 |
| | 23 | 17 | 40 | 39 |
| | 47 | 18 | 38 | 28 |
| | 43 | 27 | 37 | 20 |
| | 41 | 27 | 34 | 20 |
| | 38 | 24 | 32 | 30 |
| | 4 | 36 | 21 | 24 |
| | 40 | 46 | 22 | 14 |
| | 49 | 45 | 21 | 15 |
| | [a]27 | 7 | 50 | 40 |
| 870 °C | 34 | 8 | 48 | 38 |
| | 48 | 11 | 45 | 34 |
| | 51 | 11 | 45 | 37 |
| | 21 | 40 | 36 | 5 |
| | 46 | 46 | 28 | 6 |
| | 29 | 24 | 39 | 21 |
| | 20 | 32 | 27 | 21 |
| | 39 | 46 | 25 | 13 |
| | [a]52 | 10 | 45 | 36 |

[a]Not cycled to failure

TABLE III. - EXPERIMENTAL DATA - 760 °C

| Specimen number | E (20 °C), GPa | E (760 °C), GPa | $\Delta\varepsilon_p$, percent[a] | $\Delta\varepsilon_t$, percent[a] | $\Delta\sigma$, MPa[a] | $\sigma_m$, MPa[a] | $N_f$ [b] |
|---|---|---|---|---|---|---|---|
| 32 | 121 | 97 | 0.074 | 1.83 | 1700 | 38 | 77 |
| 25 | 134 | 108 | .287 | 1.91 | 1760 | 54 | 36 |
| 14 | 255 | 211 | .078 | 1.00 | 1940 | -23 | 47 |
| 45 | 239 | 198 | .074 | 0.89 | 1620 | -38 | 137 |
| 19 | 158 | 121 | .220 | 1.41 | 1440 | -47 | 179 |
| 23 | 127 | 106 | .075 | 1.50 | 1520 | 33 | 115 |
| 47 | 142 | 115 | .075 | 1.28 | 1400 | 56 | 220 |
| 43 | 188 | 145 | .075 | 1.09 | 1480 | -22 | 328 |
| 41 | 158 | 131 | .246 | 1.40 | 1510 | -67 | 100 |
| 38 | 132 | 102 | .085 | 1.47 | 1420 | 49 | 310 |
| 4 | 195 | 203 | .090 | 0.89 | 1630 | 23 | 452 |
| 40 | 261 | 205 | .069 | 0.70 | 1300 | -10 | 550 |
| 49 | 230 | 186 | .164 | 0.95 | 1480 | -19 | 187 |

[a]Cycle parameters measured at approximately $N_f/2$.
[b]$N_f$ is defined as total failure or a 10 percent drop in tensile load.

TABLE IV. - EXPERIMENTAL DATA - 870 °C

| Specimen number | E (20 °C), GPa | E (870 °C), GPa | $\Delta\varepsilon_p$, percent[a] | $\Delta\varepsilon_t$, percent[a] | $\Delta\sigma$, MPa[a] | $\sigma_m$, MPa[a] | $N_f$ [b] |
|---|---|---|---|---|---|---|---|
| 34 | 120 | 96 | 0.091 | 0.99 | 862 | 59 | 1856 |
| [c]48 | 117 | 92 | .110 | 1.18 | 986 | 47 | 1003 |
| 51 | 110 | 87 | .100 | 1.23 | 986 | 47 | 1501 |
| [c]21 | 247 | 185 | .100 | 0.72 | 1150 | 93 | 630 |
| 46 | 200 | 150 | .110 | 0.90 | 1190 | 82 | 484 |
| 29 | 165 | 121 | .098 | 0.99 | 1080 | 24 | 1502 |
| 20 | 199 | 137 | .098 | 0.87 | 1060 | -34 | 859 |
| 39 | 174 | 136 | .103 | 0.91 | 1100 | 115 | 552 |

[a]Cycle parameters measured at approximately $N_f/2$.
[b]$N_f$ is defined as total failure of a 10 percent drop in tensile load.
[c]Due to an experimental error, specimen numbers 48 and 21 were cycled at a positive mean strain of approximately 0.10 percent.

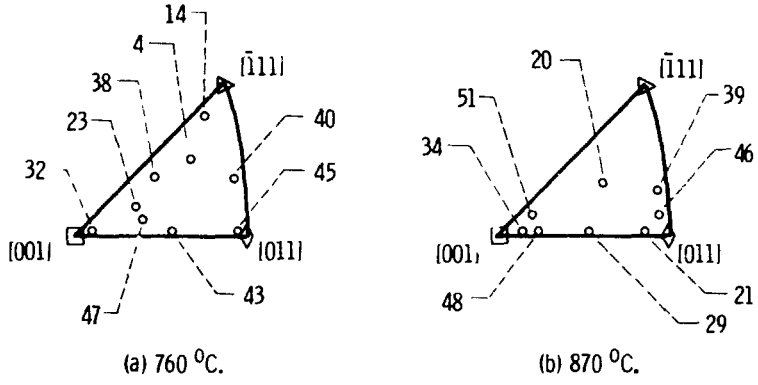


(a) 760 °C. (b) 870 °C.

Figure 1. - Approximate tensile axis orientations, with specimen numbers indicated.

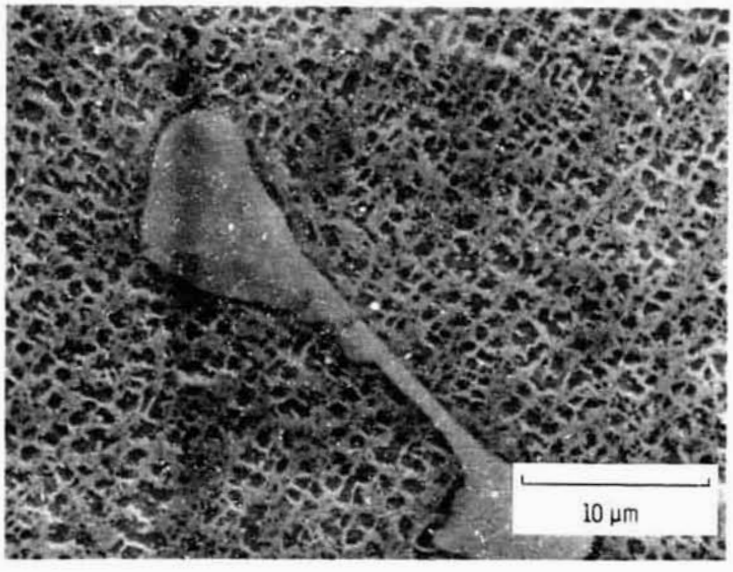


(a) SEM micrograph of an interdendritic region, including a large MC type carbide.

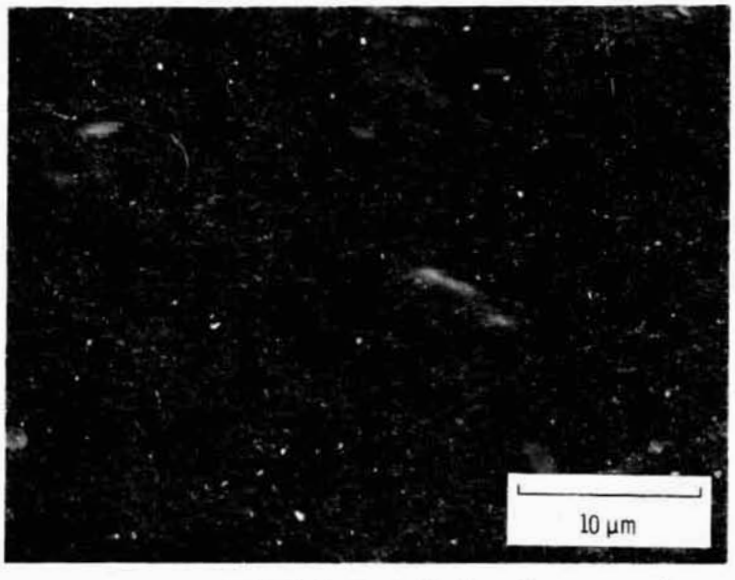


(b) SEM micrograph of a dendrite core region from the same specimen.

Figure 2. - Initial microstructure.

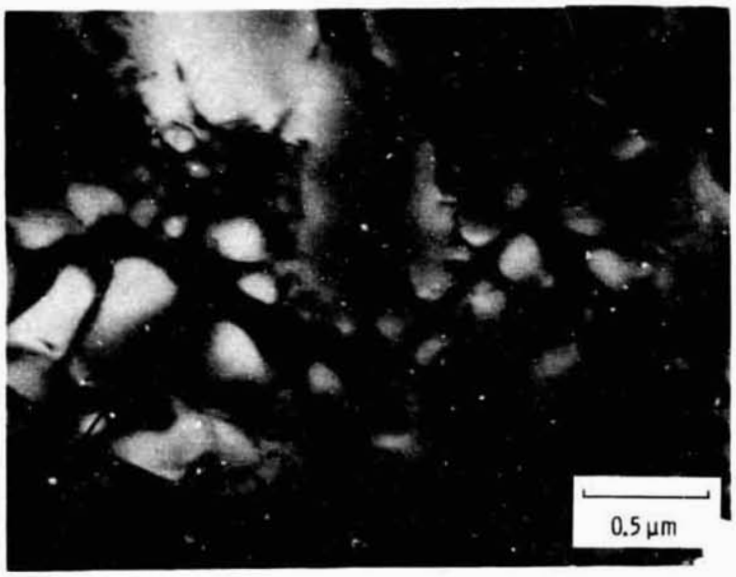


(c) TEM darkfield micrograph of the same specimen, using the <300> reflection.

Figure 2. - Concluded.

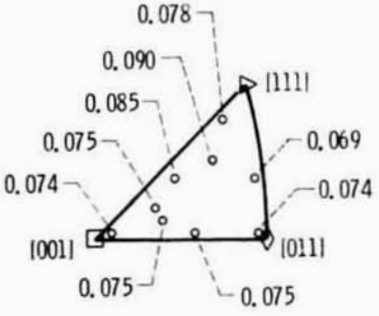


(a) $\Delta\varepsilon_p$ [%].

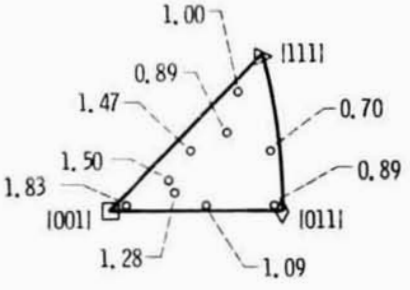


(b) $\Delta\varepsilon_t$ [%].

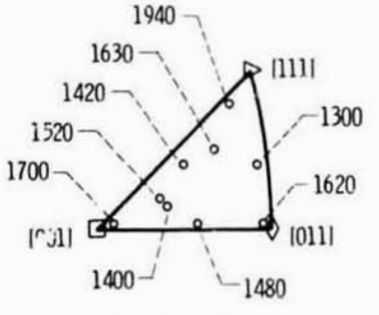


(c) $\Delta\sigma$ [MPa].

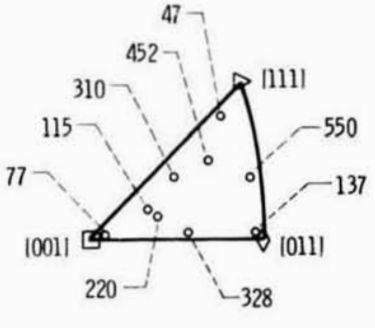


(d) $N_f$.

Figure 3. - Fatigue test parameters for the 760 °C, low $\Delta\varepsilon_p$ tests, measured at approximately $N_f/2$.

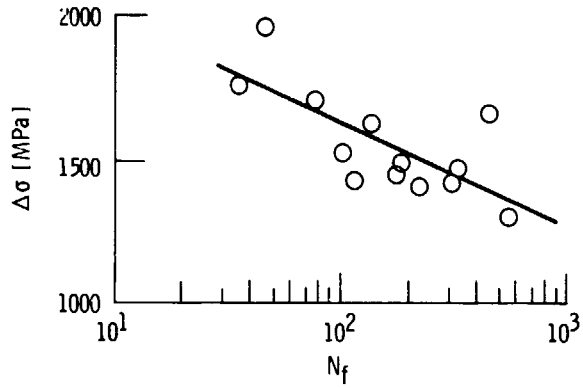


Figure 4. - $\Delta\sigma/N_f$ representation of the 760 $^{o}$C data.

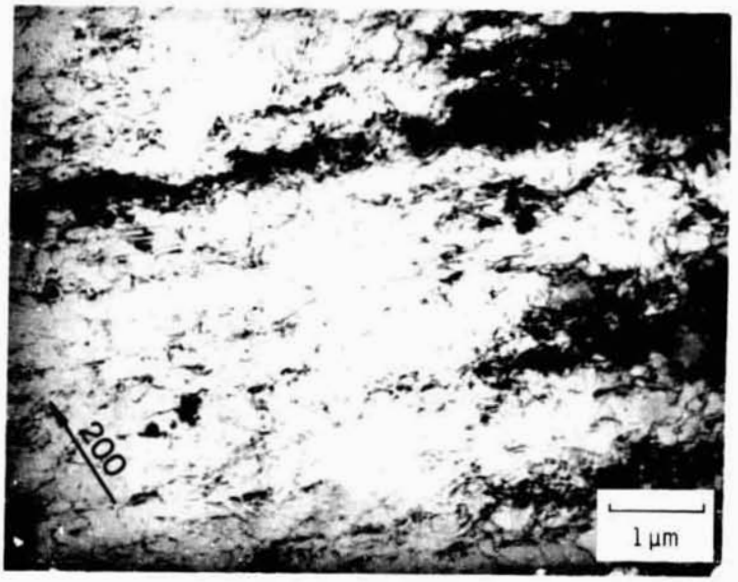


(a) #23 (single slip orientation).

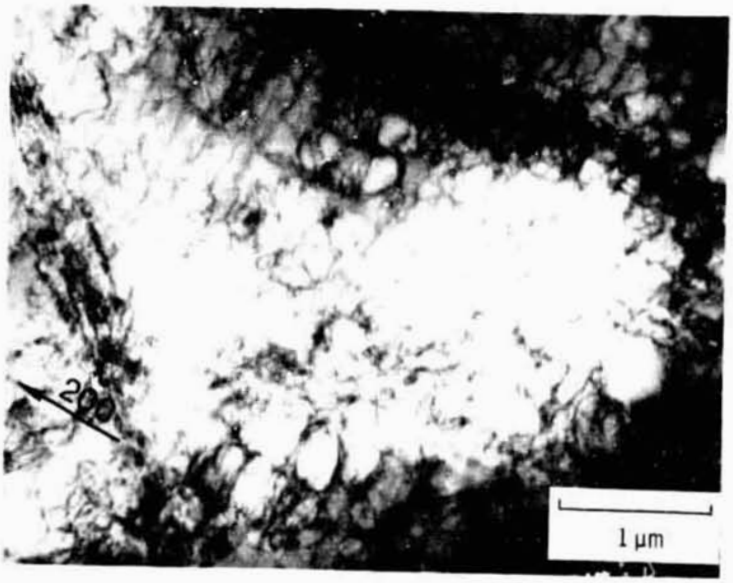


(b) #27 (<001> orientation, not cycled to failure).

Figure 5. - TEM micrographs of the deformation microstructure after fatigue at 760 $^{o}$C.

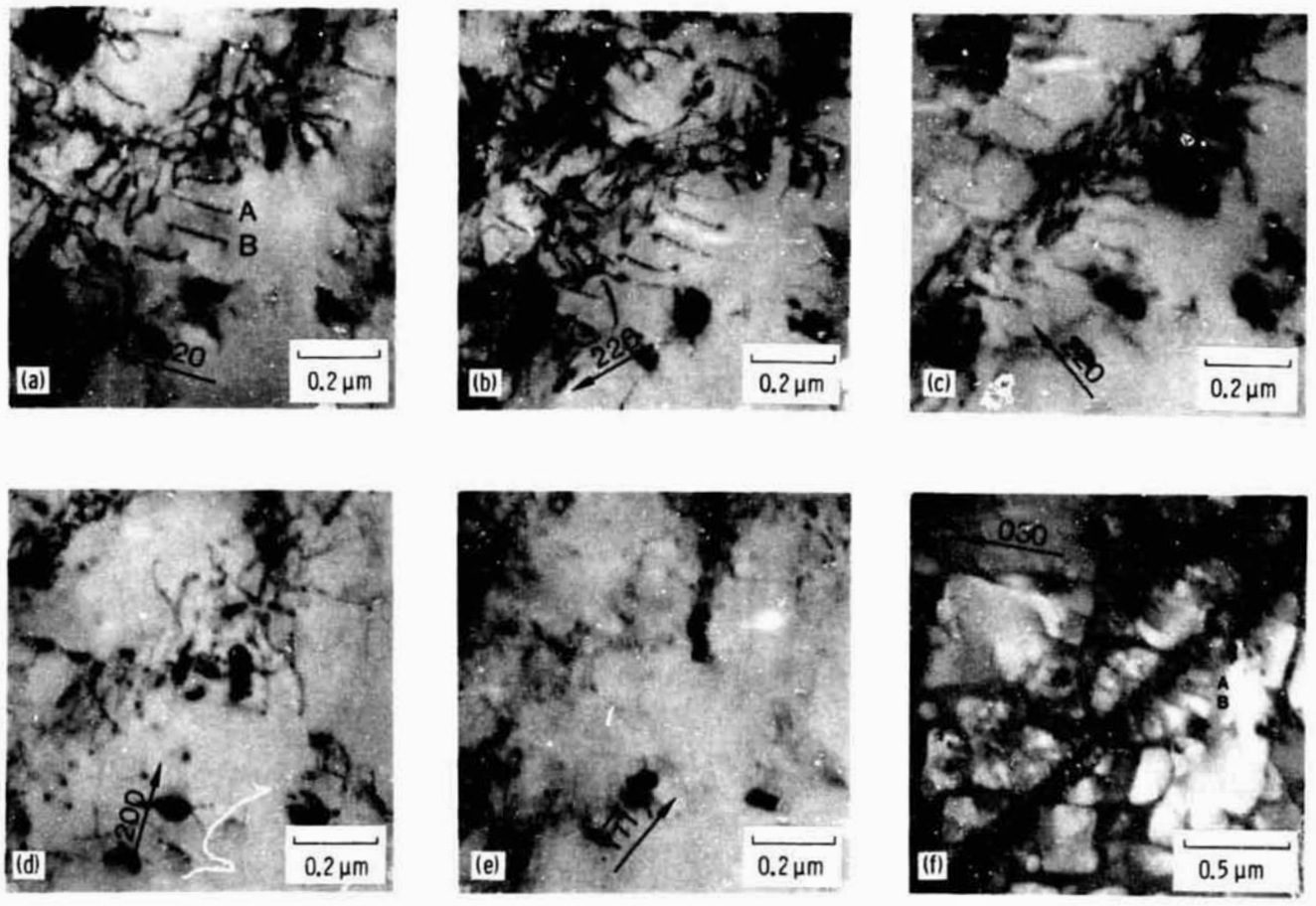


Figure 6. - TEM micrographs of slip band in specimen #27 (<001> cycled at 760 $^{0}$C) under different operating reflections. The dislocations marked A and B lie on the cube cross-slip plane, while the dislocations in the band lie on octrahedral planes.

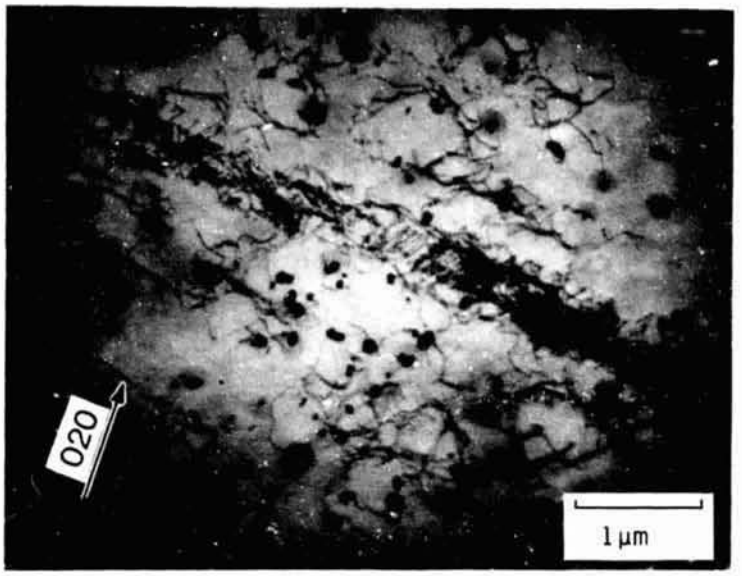


(a) <020> reflection.

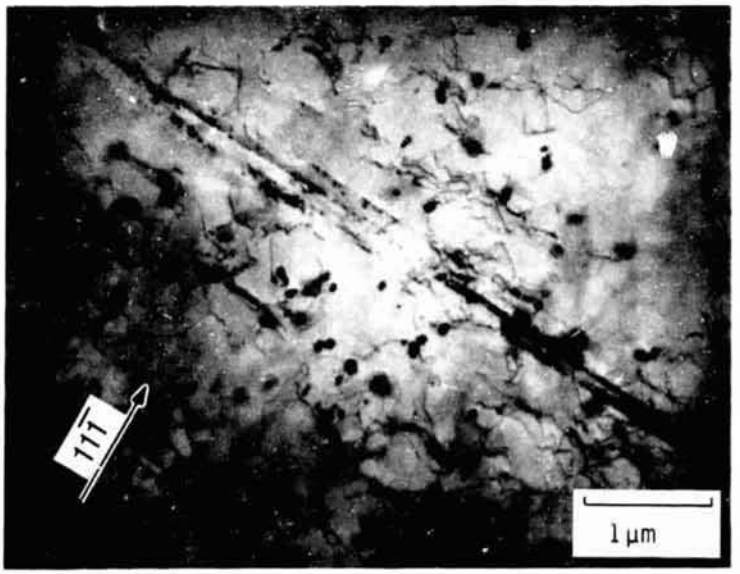


(b) <111> edge-on reflection, showing only residual contrast.

Figure 7. - TEM micrographs of a slip band in specimen #27 showing the planar nature of the bands.

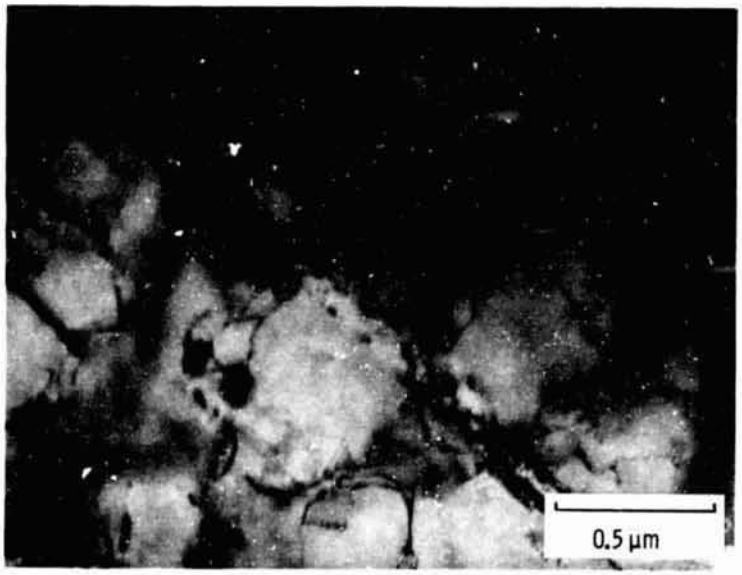


(c) <111> reflection. (The small dark particles are carbides.)

Figure 7. - Concluded.

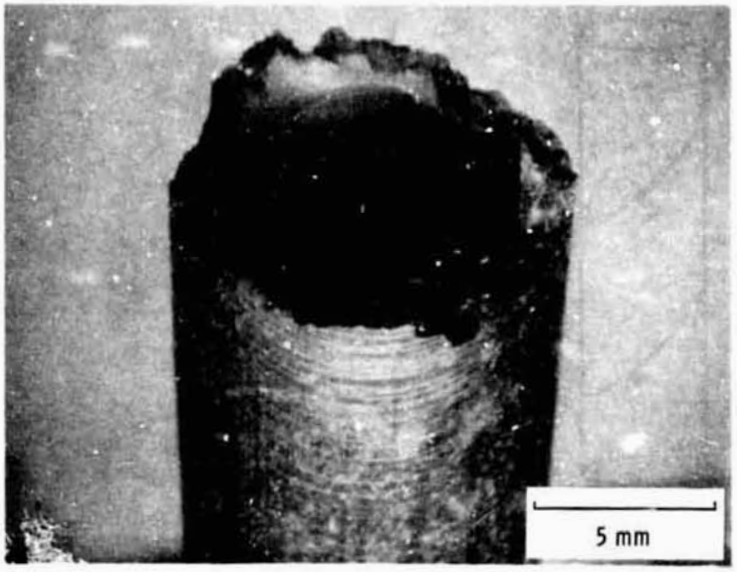


(a) Micrograph showing slip traces.

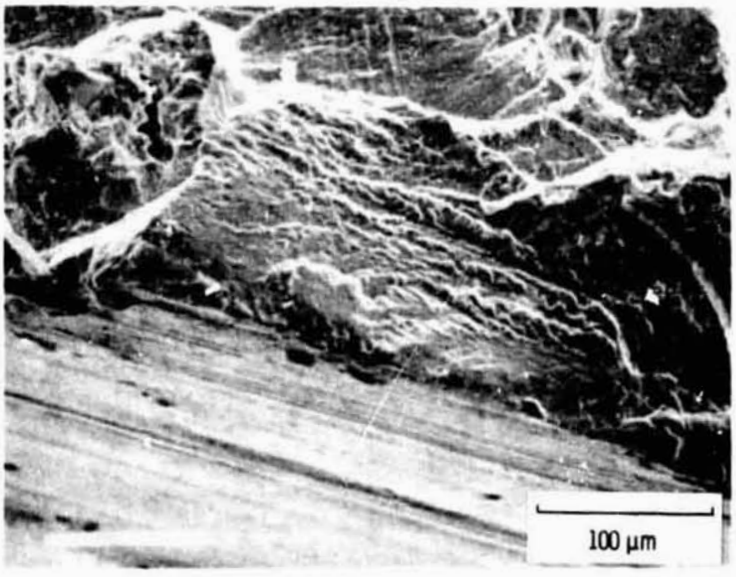


(b) SEM fractograph showing micropore crack initiation and slip traces.

Figure 8. - Specimen #43 (single slip, cycled at 760 $^{0}$C).

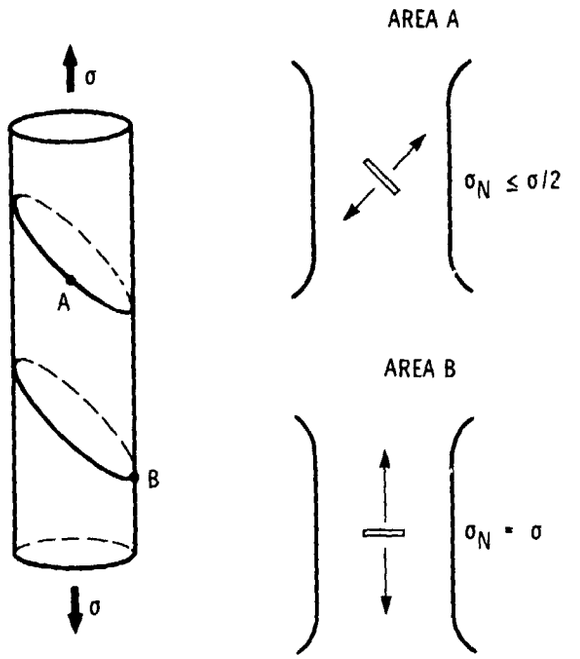


Figure 9. - Diagram showing why crack initiation was always at "Site B" in single slip crystals cycled at 760 °C.

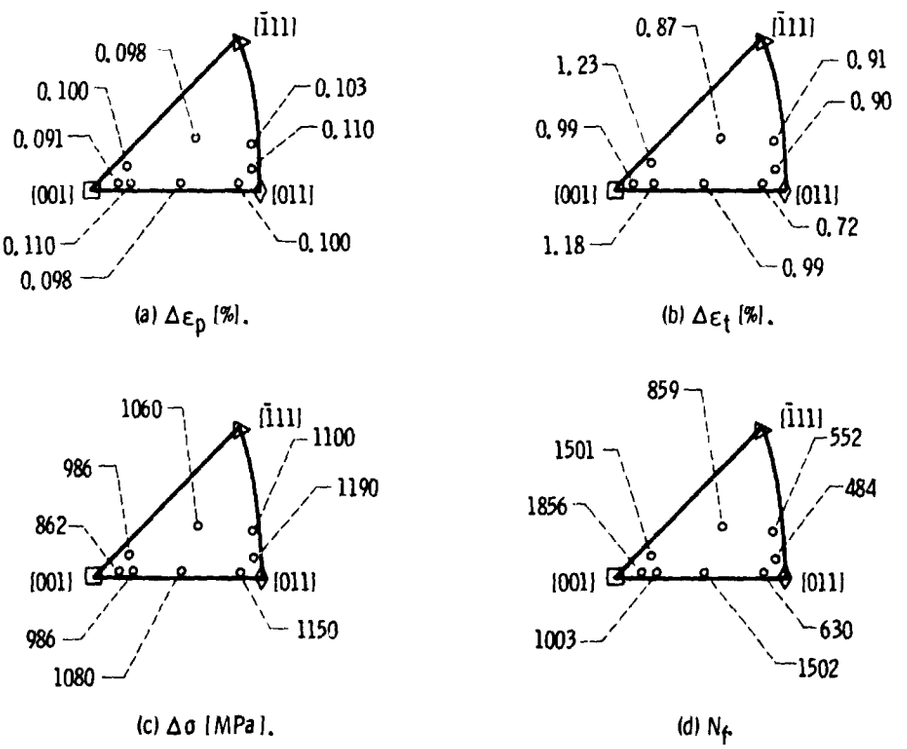


Figure 10. - Fatigue test parameters for the 870 °C tests, measured at approximately $N_f/2$.

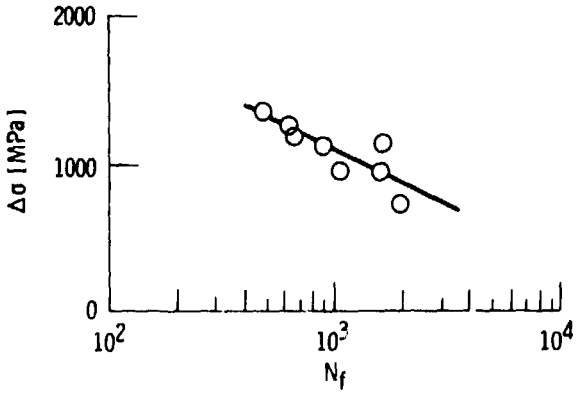


Figure 11. - $\Delta\sigma/N_f$ representation of the 870 °C data.

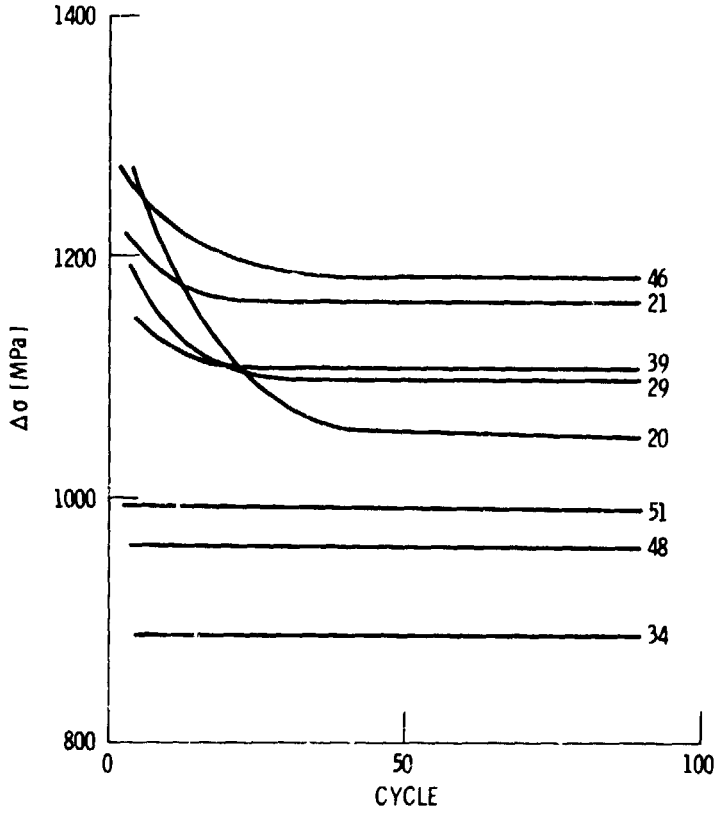


Figure 12. - Plot of $\Delta\sigma$ versus cycle at 870 °C.

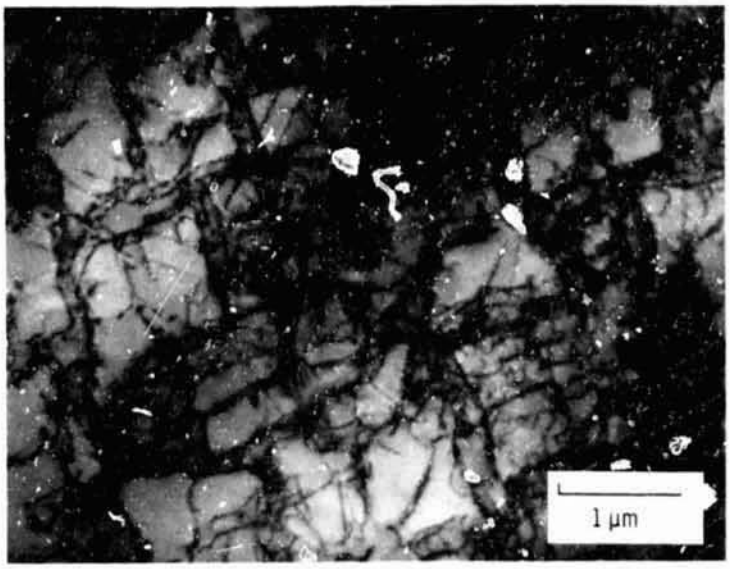


(a) Brightfield.

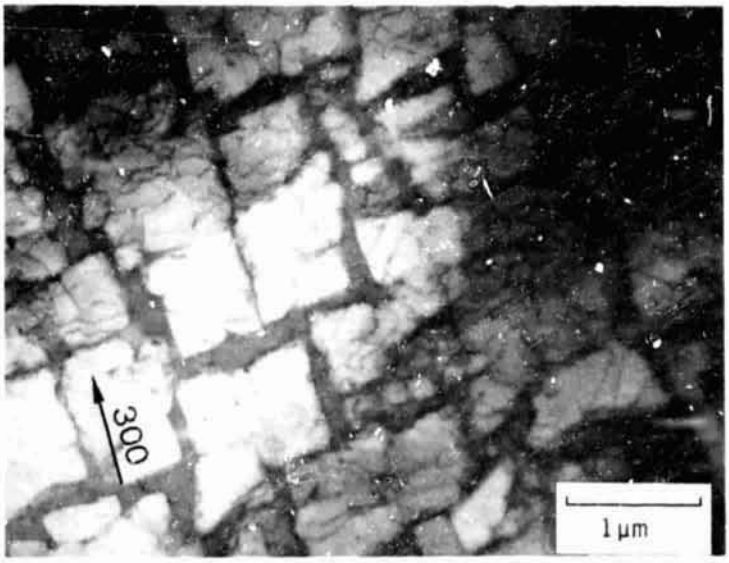


(b) Darkfield of same area, slightly translated.

Figure 13. - TEM micrographs of specimen #48 (<001>cycled at 870 $^{0}$C).

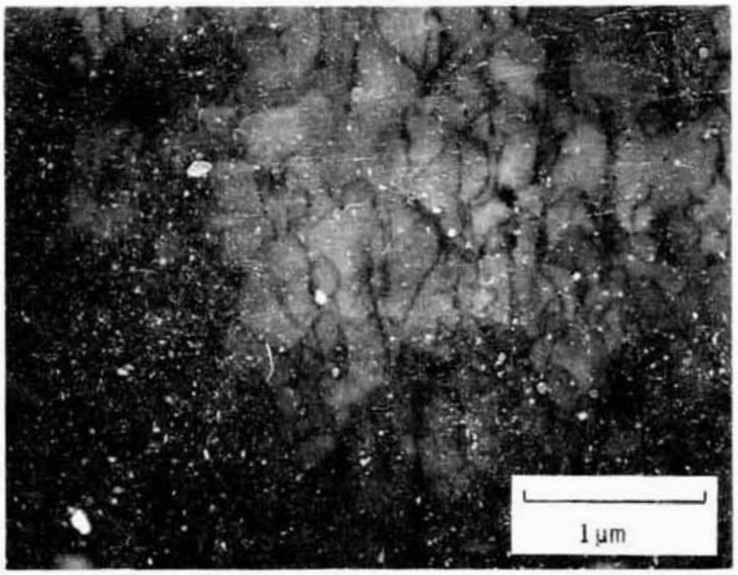


Figure 14. - TEM micrograph of specimen #21 (<011>cycled at 870 $^{0}$C).

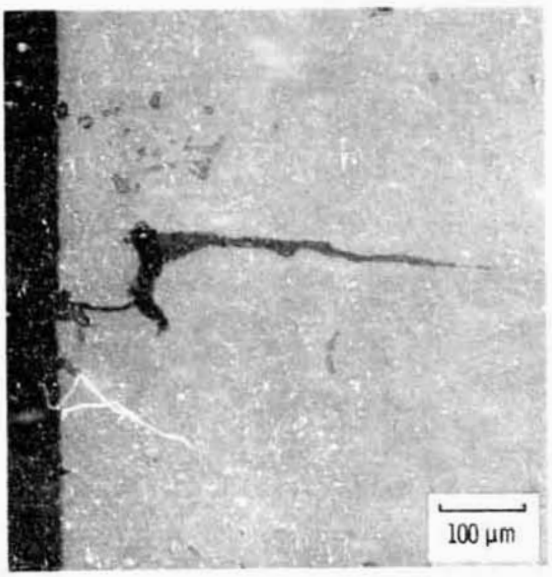


(a) Micrograph, specimen #39, unetched.

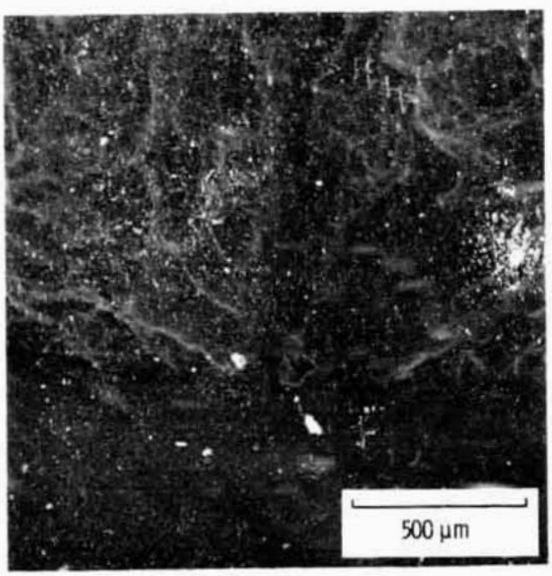


(b) SEM fractograph, specimen #29.

Figure 15. - Crack initiation at micropores at 870 $^{o}$C.

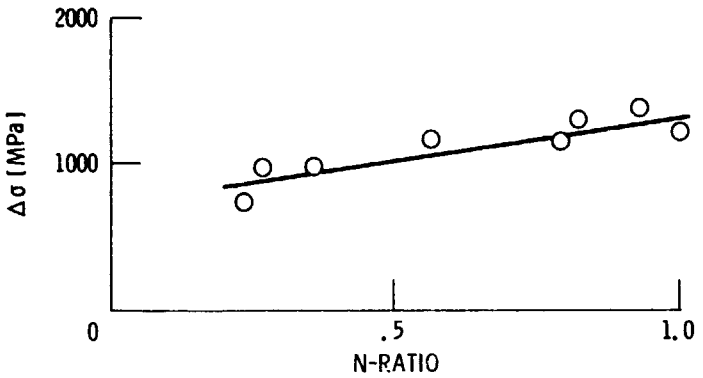


Figure 16. - Plot of $\Delta\sigma$ versus N at 870 °C.
$N = (M_{[\bar{1}01](010)})/(M_{[\bar{1}01](111)})$ [Ref. 16].

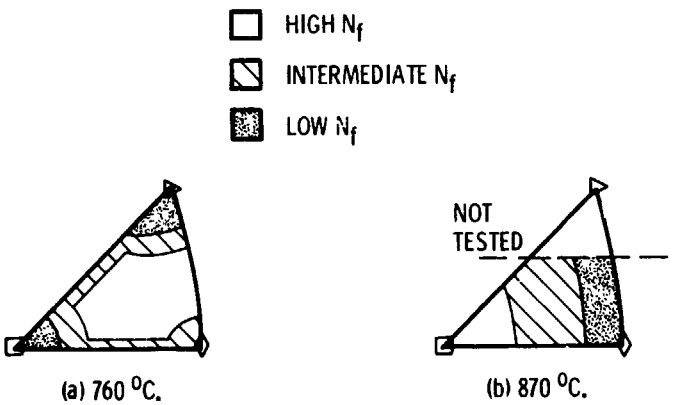


Figure 17. - Illustration of the orientation dependence of fatigue lives for a constant plastic strainrange at 760 and 870 °C.